Chinese Chemical Letters 35 (2024) 108309

Contents lists available at ScienceDirect

Chinese Chemical Letters

journal homepage: www.elsevier.com/locate/cclet

Understanding AIE and ACQ phenomenon of organometallic iridium(III) complexes by simple cationization engineering

Weilin Song[a,1], Huiting Mao[a,d,1], Ying Gao[b,*], Yaxuan Yao[c], Guo-Gang Shan[c,*], Zhongmin Su[a,*]

[a] State Key Laboratory of Supramolecular Structure and Materials, Institute of Theoretical Chemistry, College of Chemistry, Jilin University, Changchun 130021, China
[b] Jilin Provincial Key Laboratory of Straw Based Functional Materials, Institute for Interdisciplinary Biomass Functional Materials Studies, Jilin Engineering Normal University, Changchun 130052, China
[c] Institute of Functional Material Chemistry and National & Local United Engineering Lab for Power Battery, Faculty of Chemistry, Northeast Normal University, Changchun 130024, China
[d] College of Life Science, Dalian Minzu University, Dalian 116600, China

ARTICLE INFO

Article history:
Received 13 January 2023
Revised 23 February 2023
Accepted 6 March 2023
Available online 1 June 2023

Keywords:
Aggregation induced-emission
Cationic iridium(III) complex
Counterion
Mechanochromic luminescence
Cell imaging

ABSTRACT

Understanding the relationship between structure and properties is critical to the development of solid-state luminescence materials with desired characteristics and performance optimization. In this work, we elaborately designed and synthesized a pair of mononuclear iridium(III) complexes with similar structures but different degrees of cationization. [Ir2-*f*][$2PF_6$] with two counterions is obtained by simple N-methylation of the ancillary ligand of [Ir1-*f*][PF_6] which is a classic cationic iridium(III) complex. Such a tiny modification results in tremendously different optical properties in dilute solutions and powders. [Ir1-*f*][PF_6] exhibits weak light in solution but enhanced emission in solid-state as well as poly(methyl methacrylate) matrix, indicative of its aggregation-induced emission (AIE) activity. On the sharp contrary, [Ir2-*f*][$2PF_6$] is an aggregation-caused quenching (ACQ) emitter showing strong emission in the isolated state but nearly nonemissive in aggregation states. Benefiting from the appealing characteristics of mechanochromic luminescence and AIE behavior, [Ir1-*f*][PF_6] has been successfully applied in reversible re-writable data recording and cell imaging. These results might provide deep insights into AIE and ACQ phenomenon of iridium(III) complexes and facilitate the development of phosphorescent materials with promising properties.

Organic luminescent materials (OLMs) have attracted much attention due to their great potential in various fields such as bioimaging [1–6], fluorescent probes [7–11], and optoelectronic devices [12–15]. The conventional OLMs, however, usually encounter emission quenching at high concentrations or in the aggregated state. This phenomenon of "aggregation-caused quenching" (ACQ) greatly hinders the development and practical applications [16]. In 2001, Tang *et al.* discovered an abnormal aggregation-induced emission (AIE) phenomenon, that is, molecules exhibiting AIE properties show no or are weak luminescent in solution but highly emissive when aggregated into nanoparticles or in the solid state [17]. It has been unveiled that the emission enhancement originated from the restriction of the intermolecular motion and disruption in close packing due to twisted geometry in the condensed phase [18,19]. In the past decades, significant efforts have been made to develop fluorescent AIE materials including molecular design, mechanism study and potential applications [20–28]. In contrast, the study on phosphorescent AIE materials is still in its infancy due to a lack of clear design principles, despite phosphors holding some advantages over fluorescent counterparts [8,29-31].

Recent research has focused on the phosphorescent iridium(III) complexes owing to the high efficiencies endowed by the strong spin-orbit coupling effect of the central iridium(III) atom [32–34]. Relatively short exited-state lifetimes, excellent photo- and thermal stabilities and tunable emission properties that can be chemically modified by altering the employed ligands endow iridium(III) complexes highly applicable for bioimaging, photocatalysis and organic electroluminescent devices [35–47]. It is believed that integrating AIE characteristics in iridium(III) complexes would be an important step for their development as multifunctional materials [48]. To date, some mononuclear and multinuclear iridium(III)

* Corresponding authors.
E-mail addresses: gaoy029@163.com (Y. Gao), shangg187@nenu.edu.cn (G.-G. Shan), zmsu@nenu.edu.cn (Z. Su).
[1] These authors contribute equally to this work.

https://doi.org/10.1016/j.cclet.2023.108309
1001-8417/

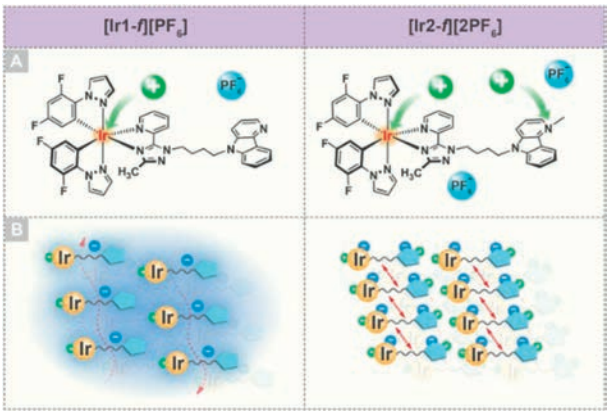

Fig. 1. (A) Chemical structures of [Ir1-*f*][PF_6] and [Ir2-*f*][$2PF_6$]. (B) Schematic illustration of molecular packing tuning by changing numbers of counterions.

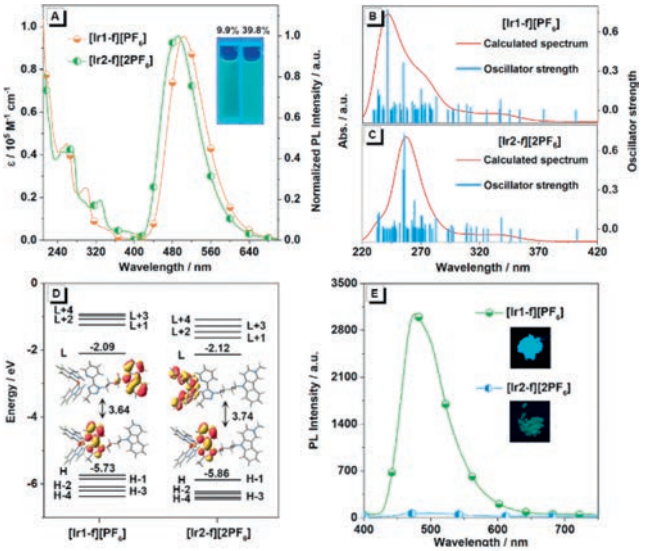

Fig. 2. (A) Absorption and photoluminescence spectra of [Ir1-*f*][PF_6] and [Ir2-*f*][$2PF_6$] in CH_3CN solution. Inset: photos of two luminogens in CH_3CN taken under the illumination of a 365 nm UV lamp. Simulated absorption spectra of complexes (B) [Ir1-*f*][PF_6] and (C) [Ir2-*f*][$2PF_6$] in CH_3CN. (D) Frontier electronic levels and surface distributions of HOMO and LUMO orbitals for complexes [Ir1-*f*][PF_6] and [Ir2-*f*][$2PF_6$]. H and L denote the HOMO and LUMO, respectively. (E) PL spectra of complexes [Ir1-*f*][PF_6] and [Ir2-*f*][$2PF_6$] in the solid state. Inset: photos of the two luminogens in the solid state taken under the illumination of a 365 nm UV lamp.

complexes with AIE properties have been reported and exhibit enhanced performances in various fields [49]. Therefore, the key to the development of AIE-active iridium(III) complexes is a clear understanding of the relationship between structure and phosphorescent property, which is highly desired for the mechanism study and controllable molecular design.

Considering the electrostatic interaction, such as which is between the emitting cationic and counterion, can not only affect the solid-state packing but also turn the corresponding excited-state characteristic [9,50]. The transformation from ACQ to AIE has been easily achieved *via* a molecular engineering strategy. For example, Wang *et al.* demonstrated that the organic dyes with a counterion effectively regulate intermolecular packing to achieve a significant improvement in photophysical performance compared to their analogues without counterions [30,51]. It is thus speculated that precise control of molecular packing by adjusting the ability of electrostatic interaction can pave a feasible way to understanding how the packing affects the emission behavior. Keeping this in mind, in this work, a pair of structurally similar mononuclear iridium(III) complexes, [Ir1-*f*][PF_6] and [Ir2-*f*][$2PF_6$], were rationally designed and synthesized (Fig. 1A). [Ir2-*f*][$2PF_6$] with two counterions was simply obtained by N-methylation of the ancillary ligand of [Ir1-*f*][PF_6] that is a classic cationic iridium(III) complex. [Ir1-*f*][PF_6] and [Ir2-*f*][$2PF_6$] were identified as AIE and ACQ molecules, respectively. The photophysical and theoretical data supported that both complexes exhibit emission with charge transfer characters in solution. Possible intraligand charge-transfer character was responsible for the weak emission of [Ir1-*f*][PF_6], while the emission of [Ir2-*f*][$2PF_6$] originated from metal-to-ligand charge-transfer (MLCT) mixed with ligand-to-ligand charge transfer (LLCT) characters that usually emit strong light in the isolated state [52,53]. Upon going from solution to solid state, however, the intermolecular interaction plays an important role in the luminescence efficiency. Due to the presence of two counterions, the relatively strong interactions weaken the emission of [Ir2-*f*][$2PF_6$] in solid-state, while [Ir1-*f*][PF_6] possesses the moderate intermolecular interaction that restricts the intermolecular motion and reduces the nonradiative channels to some extent, leading to enhanced emission (Fig. 1B). Reversible re-writable data recording device and cell imaging using [Ir1-*f*][PF_6] as media were developed with the merits of mechanochromic luminescence (MCL) and AIE properties.

The detailed synthetic routes and characterization of target complexes [Ir1-*f*][PF_6] and [Ir2-*f*][$2PF_6$] as well as the used ligands in this work can be found in Scheme S1, Figs. S1-S6 and Experimental section (Supporting information) [54,55]. Fig. 2A depicts the absorption spectra of complexes [Ir1-*f*][PF_6] and [Ir2-*f*][$2PF_6$] in CH_3CN solution with the concentration of 1×10^{-5} mol/L at room temperature under the ambient atmosphere. Complexes [Ir1-*f*][PF_6] and [Ir2-*f*][$2PF_6$] show intense absorption bands in the ultraviolet region (<280 nm), which can be ascribed to the spin-allowed ligand-centered $^1\pi$-π^* transition, involving both the cyclometalated and ancillary ligands. In addition, the moderate bands within the scope of 290–340 nm originate from the spin-allowed MLCT and LLCT [56]. Beyond 340 nm, the long tail absorption can be assigned to the mixed transitions of the spin-forbidden ^{3}MLCT/^{3}LLCT or $^3\pi$-π^* transitions. The spin-forbidden triplet transitions could be partially broken by the strong spin-orbit coupling of the heavy iridium(III) center. Theoretical calculations were performed to understand the excited states involved in the absorption spectra using Gaussian 09 program package [57]. The simulated UV–visible absorption spectra of both complexes were depicted in Figs. 2B and C. TD-DFT results can reproduce well the main bands observed in the experimental spectra profiles. Fig. 2D displays the optimized ground state (S_0) geometries along with the energy levels and surface distributions of the highest occupied molecular orbital (HOMO) and lowest unoccupied molecular orbital (LUMO). Illustrations on more molecular orbitals are presented in Figs. S7 and S8 and the data are listed in Tables S1 and S2 (Supporting information). According to the absorption bands assignment details in Supporting information, the calculated transition characteristics are coincided with the experimental results.

The photoluminescence spectra (PL) of complexes [Ir1-*f*][PF_6] and [Ir2-*f*][$2PF_6$] at 298 K in acetonitrile are depicted in Fig. 2A. The luminescence properties and photophysical parameters of them in different states were measured and the data were depicted in Table 1. In line with the absorption spectra, complex [Ir1-*f*][PF_6] and [Ir2-*f*][$2PF_6$] show similar emission properties with broad and structureless bands with an emission centered at 504 and 492 nm, respectively, which indicates the charge-transfer character involved in their emitting triplet states in the CH_3CN solution [53]. The excited-state lifetimes of complexes [Ir1-*f*][PF_6] and [Ir2-*f*][$2PF_6$] in degassed CH_3CN solutions were estimated to be 0.14 and 0.01 μs, respectively, confirming the phosphorescence origin of the emissions (Fig. S9 and Table 1 in Supporting infor-

Table 1
Photophysical and electrochemical characteristics for complexes [Ir1-*f*][PF_6] and [Ir2-*f*][$2PF_6$].

Complexes	Emission		PLQY		τ	
	λ_{em} (nm)		Φ_{em} (%)		τ (μs)	
[Ir1-*f*][PF_6]	504[a]	477[b]	9.9[a]	43.7[b]	0.14[a]	0.43[b]
[Ir2-*f*][$2PF_6$]	492[a]	501[b]	39.8[a]	0.5[b]	0.01[a]	0.02[b]

[a] Measured in the degassed CH_3CN solution (10^{-5} mol/L) at 298 K.
[b] Measured in the solid powder state at 298 K.

mation) [58]. Meanwhile, complexes [Ir1-*f*][PF_6] and [Ir2-*f*][$2PF_6$] give photoluminescent quantum yields (PLQY) of 9.9% and 39.8% in the solution, respectively (Table 1). To provide a deeper understanding of the different emissive characteristics, the lowest triplet states (T_1) of both complexes were studied (Fig. S10 in Supporting information). After full-geometry relaxation of T_1, it is found that the spin-density distribution calculated for [Ir1-*f*][PF_6] (Ir, 0.008e; triazole-pyridine moiety, 0.84e; pyrido[4,3-*b*]indole, 0.97e) and [Ir2-*f*][$2PF_6$] (Ir, 0.43e; cyclometalated ligand, 0.55e; ancillary ligand, 1.01e) perfectly matches the topology of the HOMO→LUMO excitation. The complex [Ir2-*f*][$2PF_6$], therefore, originates an admixture of ^{3}MLCT and ^{3}LLCT character, which is consistent with the stronger emission spectrum of [Ir2-*f*][$2PF_6$] in solution. Nevertheless, the charge transfer of complex [Ir1-*f*][PF_6] occurs only between the carboline fraction and 1,2,4-triazole group in the ancillary ligand. Consequently, it is suggested that the emissive excited state of [Ir1-*f*][PF_6] has a predominantly intraligand charge-transfer (^{3}ILCT) character, explaining why [Ir1-*f*][PF_6] shows weak emissions in the dilute solution [53]. In sharp contrast, complex [Ir1-*f*][PF_6] exhibits much higher PL intensity (Fig. 2E) with PLQY of 43.7% in solid state compared with that of complex [Ir2-*f*][$2PF_6$] with a value of only 0.5% (Table 1). The results indicate that cationization engineering may be a feasible way to adjust the emission behaviors of iridium(III) complexes, and also suggest that the counterion has a significant effect on the molecular packing in the solid state.

Considering the different emission features between dilute solutions and solid states, systematic investigations on the aggregation formation of complexes [Ir1-*f*][PF_6] and [Ir2-*f*][$2PF_6$] were also conducted. Fig. 3A shows the luminescent photographs of complexes [Ir1-*f*][PF_6] and [Ir2-*f*][$2PF_6$] in the CH_3CN-water solution under handheld UV illumination (365 nm) with different water fractions (f_w, volume percentage of water in water/CH_3CN mixtures) added. Clearly, complex [Ir1-*f*][PF_6] exhibits typical AIE optical characteristics, while complex [Ir2-*f*][$2PF_6$] shows classic ACQ property, further demonstrated by the comparison of their fluorescence spectra (Figs. 3B and C). As shown in Fig. 3D, the emission intensity of complex [Ir1-*f*][PF_6] gradually increases when the poor solvent (water) was added to the CH_3CN solution. Obviously, for mixtures with a high content of water (f_w = 90%), the PL intensity of complex [Ir1-*f*][PF_6] is stronger than that in pure CH_3CN solution. With the further addition of water, however, [Ir2-*f*][$2PF_6$] shows a steady decrease in emission intensity and finally attained the base level (Fig. 3D). It is noteworthy that the slight red shift observed with the increased f_w for [Ir1-*f*][PF_6], which could result from the changes of intermolecular interactions and formation of nano-aggregation with the addition of water. In the case of the studied system, we infer that changing the counterions numbers of iridium(III) complexes by cationization engineering has a considerable impact on the emission properties in the solid state, that is, additional counterion will increase the intermolecular interaction of the complex, leading to weak luminescence in comparison with that in solution.

To test our above hypothesis, solution-process doped thin films with 1–50 wt% doping ratios in host polymethyl methacrylate

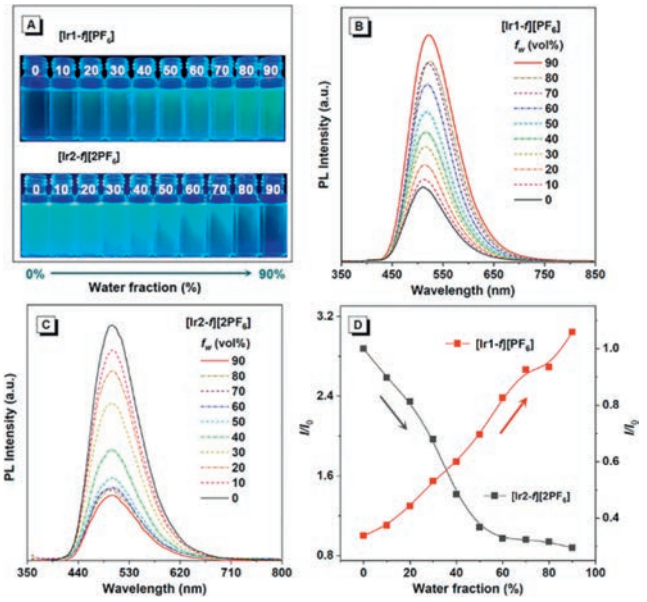

Fig. 3. (A) Luminescent photographs of solutions or suspensions of [Ir1-*f*][PF_6] and [Ir2-*f*][$2PF_6$] in water/CH_3CN mixtures with different fractions of water (f_w), with [Ir1-*f*][PF_6] and [Ir2-*f*][$2PF_6$] showing typical AIE and ACQ effects, respectively. Emission spectra of (B) [Ir1-*f*][PF_6] and (C) [Ir2-*f*][$2PF_6$] in water/CH_3CN mixtures (0–90%). (D) Plot of maximum emission intensity of [Ir1-*f*][PF_6] an d [Ir2-*f*][$2PF_6$] *versus* water fraction.

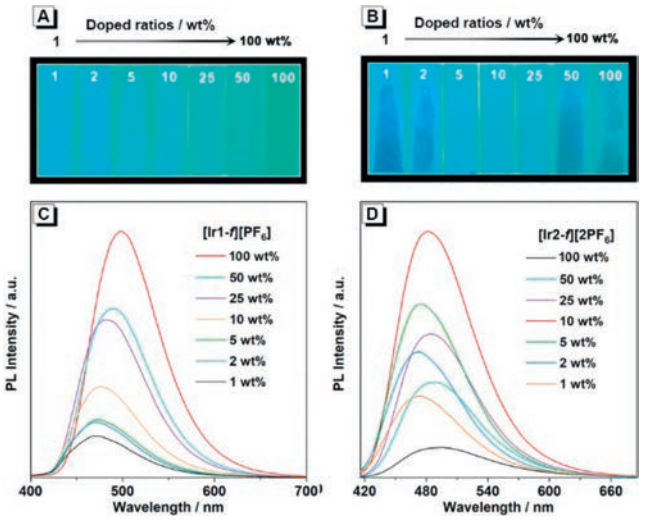

Fig. 4. Photoluminescence spectra and luminescent photographs of complexes (A, C) [Ir1-*f*][PF_6], and (B, D) [Ir2-*f*][$2PF_6$] in doped films (1–100 wt% doping concentration, PMMA as the host).

(PMMA) and neat film were prepared (Figs. 4A and B). As the doping concentration increased, the PL spectra of both complexes undergo a gradual redshift which is related to strong intermolecular interactions (Figs. 4C and D). PL intensity of thin films increases as the doping concentration of complex [Ir1-*f*][PF_6] increases from 1 wt% to 100 wt% in PMMA. On the contrary, complex [Ir2-*f*][$2PF_6$] achieves maximum PL intensity at a doped concentration of 10 wt%, and the emission is significantly weaker under the neat film. In the neat-film state where the intermolecular interactions between emitters are enhanced. Based on the above results, it is noted that complex [Ir2-*f*][$2PF_6$] with two counterions may increase the intermolecular interaction, thereby inducing luminescence quenching in the aggregate state.

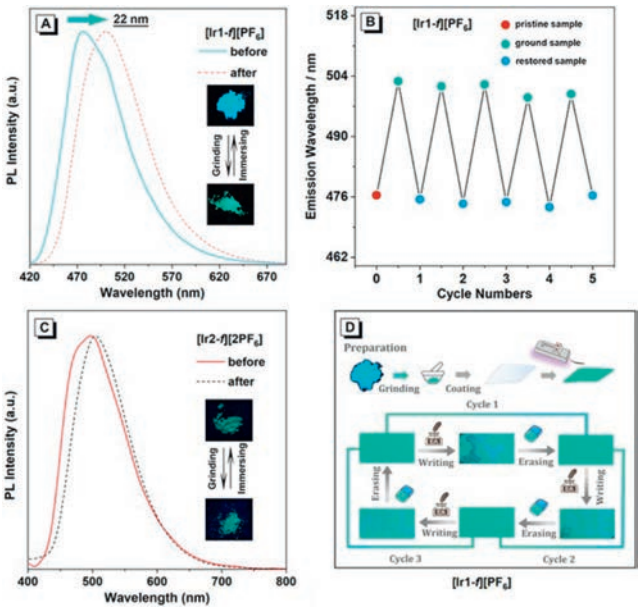

Fig. 5. Emission spectra of (A) [Ir1-*f*][PF_6] and (C) [Ir2-*f*][$2PF_6$] before and after grinding. (B) The repeated cycles of the grinding and recovery processes for complex [Ir1-*f*][PF_6]. (D) A reversibly rewritable data recording device based on complex [Ir1-*f*][PF_6].

The change in solid-state emission of complexes [Ir1-*f*][PF_6] and [Ir2-*f*][$2PF_6$] was monitored by applying mechanical force by means of a mortar and pestle. Under 365 nm UV lamp, the pristine of [Ir1-*f*][PF_6] shows sky blue phosphorescence with emission peak of 477 nm. Upon grinding treatment of original solid powders in an agate mortar, a red shift of the emission by *ca.* 22 nm to λ_{max} 499 nm is observed (Fig. 5A). The ground state of [Ir1-*f*][PF_6] could be completely reverted by solvent-induced recrystallization process. Upon further grinding the sample, an obvious red-shifted emission reappeared. The whole process could be repeated at least five times, indicative of the excellent reversibility of the mechanochromism (Fig. 5B). In addition, the average lifetime of as-prepared powder of [Ir1-*f*][PF_6] changes from 0.43 μs to 1.02 μs (Fig. S11 in Supporting information). However, no obvious MCL phenomenon and the change of τ values are observed for [Ir2-*f*][$2PF_6$] (Fig. 5C). The distinctly opposite phenomenon of two complexes before and after grinding indicates that the molecular packing and intrinsic exited-state characteristic of cationic iridium(III) complexes play a key role in deciding the emission behaviors in pristine as well as ground solid-state powders.

To understand the origin and mechanism of the MCL behaviors of these complexes, the powder X-ray diffraction (PXRD) patterns of [Ir1-*f*][PF_6] and [Ir2-*f*][$2PF_6$] before and after grinding were carried out. As presented in Fig. S12 (Supporting information), the original solids of both complexes display intense and sharp reflection peaks, which indicates their well-ordered crystalline phase. In contrast, these diffraction peaks become weaker and broader after grinding for two complexes, which represents the significant damage of the crystalline state and the formation of a partial amorphous state in the ground form. However, complex [Ir2-*f*][$2PF_6$] exhibited insignificant MCL activity, although the physical phase transition also changed from the crystalline to the amorphous state during grinding. To further comprehend the different MCL behavior, theoretical calculations were performed to calculate the transition dipole moment from the T_1 to S_0. The transition dipole moment is related to the excited-state energy distributions of dimers, and thus influences the photophysical properties [59]. Accordingly, if there is a larger transition dipole moment achieved in a molecule, it will be more susceptible to external stimuli. Complexes [Ir1-*f*][PF_6] and [Ir2-*f*][$2PF_6$] show the transition dipole moment of 0.2988 and 0.0324 Debye, respectively, which explains the unique MCL capabilities of complexes [Ir1-*f*][PF_6]. Moreover, [Ir2-*f*][$2PF_6$] shows poor PLQY in the solid state, it is thus speculated that complex [Ir2-*f*][$2PF_6$] may possess a tighter packing than complex [Ir1-*f*][PF_6] in the solid state, which is difficult to be affected upon external force, resulting in no distinct change in emission wavelength. Instead, these relatively weak intermolecular interactions in complex [Ir1-*f*][PF_6] might be destroyed easily by mechanical stimuli and lead to stimuli-responsive behavior.

Due to the excellent MCL behavior and good reversibility of complex [Ir1-*f*][PF_6], a reversible re-writable data recording device was fabricated (Fig. 5D). The specific reversible procedure is as follows. Firstly, this complex was ground and coated on a filter paper as the 'thin film' which showed green emission under UV excitation. Then, the word 'Ir' was written using a specially made 'pen' which was made of a cotton bud with ethyl acetate as the 'ink'. Due to the change of emission color, the blue emitting could be visible. Following that, the 'Ir' could be erased by grinding to make it completely disappear, resulting in the recovery of the initial green thin film. A new word 'AIE' could be written again with the 'pen' of the ethyl acetate solvent, which could still be removed by grinding. The entire writing and erasing processes could be repeated multiple times, another new word 'MCL' could be written on the 'thin film' for the third time and erased according to the method described above. The above process is supported by a change in the crystal phase before and after writing in ink. As a consequence, we envision that complex [Ir1-*f*][PF_6] have great potential for optical data recording and security protection.

Based on the excellent photophysical properties of complex [Ir1-*f*][PF_6], we then investigated its potential for bioimaging. To improve the biocompatibility, good water-dispersible nanoparticles ([Ir1-*f*][PF_6] NPs) were also prepared by using the 2-distearoyl-*sn*–glycero-3-phosphoethanolamine-*N*-[methoxy (polyethyleneglycol)–2000] (DSPE-mPEG-2000) (Fig. S13A in Supporting information). Cell imaging experiments were then carried out based on HeLa cells after incubation with the nanoparticle of [Ir1-*f*][PF_6], evaluated by confocal laser scanning microscopy (CLSM). The bright emission is collected from HeLa cells after incubating with the nanoparticle of [Ir1-*f*][PF_6], indicating its rapid permeability for living cells (Fig. S13A). To further prove the organelle-targeting specificity of [Ir1-*f*][PF_6] for imaging, the co-localization experiments were performed by incubating HeLa cells with Mito-Tracker Green, which are commercial specific agents mitochondria imaging, respectively. The fluorescence signal of [Ir1-*f*][PF_6] (blue) overlapped well with that of commercial Mito-Tracker Green (green) with a Pearson correlation coefficient of 0.88 (Fig. S13B in Supporting information), which indicates the complex [Ir1-*f*][PF_6] possesses specific mitochondrial targeting capability [60].

In summary, to better understand the structure-property relationship, a pair of mononuclear iridium(III) complexes [Ir1-*f*][PF_6] and [Ir2-*f*][$2PF_6$] were precisely designed by cationization engineering strategy. The detailed photophysical results demonstrate that [Ir1-*f*][PF_6] and [Ir2-*f*][$2PF_6$] exhibited AIE and ACQ phenomena, respectively. The theoretical and experimental data suggest that the ^{3}ILCT character would be the possible reason why [Ir1-*f*][PF_6] shows weak emission in solution, while the strong emission of [Ir2-*f*][$2PF_6$] should attribute to the admixture of ^{3}MLCT and ^{3}LLCT characters. In the case of solid-state, the suppressed and enhanced nonradiative decay processes caused by the local environment alteration lead to their distinct emission behavior. The reversible re-writable data recording device and cell imaging based on [Ir1-*f*][PF_6] are achieved successfully owing to its appealing mechanochromism and AIE property. The results reported herein

might provide deep insights into the AIE and ACQ phenomenon of iridium(III) complexes and would offer a generic and effective way for developing phosphorescent materials with controllable emission properties in the future.

Declaration of competing interest

The authors declare that they have no known competing financial interests or personal relationships that could have appeared to influence the work reported in this paper.

Acknowledgment

The authors gratefully acknowledge the financial support from the National Natural Science Foundation of China (Nos. 22175033 and 51902124).

Supplementary materials

Supplementary material associated with this article can be found, in the online version, at doi:10.1016/j.cclet.2023.108309.

References

[1] D.M. Mayder, R. Hojo, W.L. Primrose, et al., Adv. Funct. Mater. 32 (2022) 2204087.
[2] K. Chen, P. He, Z. Wang, et al., ACS Nano 15 (2021) 7735–7743.
[3] F. Xiao, H. Gao, Y. Lei, et al., Nat. Commun. 13 (2022) 186.
[4] G. Morselli, M. Villa, A. Fermi, et al., Nanoscale Horiz 6 (2021) 676–695.
[5] E. Bassan, A. Gualandi, P.G. Cozzi, et al., Chem. Sci. 12 (2021) 6607–6628.
[6] R. Li, J. Liu, C. Xia, et al., Chin. Chem. Lett. 34 (2023) 107900.
[7] L.J. Mei, C. Fan, C.R. Xu, et al., Chem. Eng. J. 451 (2023) 139027.
[8] Z. Mao, J. Xiong, P. Wang, et al., Coord. Chem. Rev. 454 (2022) 214356.
[9] H. Shi, H. Sun, H. Yang, et al., Adv. Funct. Mater. 23 (2013) 3268–3276.
[10] A. Fermi, G. Bergamini, M. Roy, et al., J. Am. Chem. Soc. 136 (2014) 6395–6400.
[11] V. Kachwal, I.R. Laskar, Topic Curr. Chem. 379 (2021) 1–38.
[12] Z. Yang, X. Ge, W. Li, et al., Chem. Eng. J. 442 (2022) 136219.
[13] C.E. Housecroft, E.C. Constable, Coord. Chem. Rev. 350 (2017) 155–177.
[14] X. Pang, K. Zhang, Y. Song, et al., Chem. Eng. J. 450 (2022) 137987.
[15] R. Yu, Y. Song, K. Zhang, et al., Adv. Funct. Mater. 32 (2021) 2110623.
[16] M. Chen, Y. Lan, J. Zheng, et al., Dalton Trans. 47 (2018) 8023–8031.
[17] J. Luo, Z. Xie, J.W. Lam, et al., Chem. Commun. (2001) 1740–1741.
[18] J.W. Chen, C.C.W. Law, J.W.Y. Lam, et al., Chem. Mater. 15 (2003) 1535–1546.
[19] Q. Peng, Z. Shuai, Aggregate 2 (2021) e91.
[20] J. Mei, N.L.C. Leung, R.T.K. Kwok, et al., Chem. Rev. 115 (2015) 11718–11940.
[21] S. Kanagaraj, A. Puthanveedu, Y. Choe, Adv. Funct. Mater. 30 (2019) 1907126.
[22] S. Huang, J. Ding, A. Bi, et al., Adv. Opt. Mater. 9 (2021) 2100832.
[23] W. Liu, X. Wang, R. Li, et al., ChemistrySelect 7 (2022) e202104111.
[24] B.S. Shivaji, R. Boddula, A. Saeki, et al., J. Mater. Chem. C 10 (2022) 5173–5182.
[25] G.J. Liu, S.N. Tian, C.Y. Li, et al., ACS Appl. Mater. Interfaces 9 (2017) 28331–28338.
[26] D. Sengottuvelu, V. Kachwal, P. Raichure, et al., ACS Appl. Mater. Interfaces 12 (2020) 31875–31886.
[27] J. Hwang, P. Nagaraju, M.J. Cho, et al., Aggregate 3 (2022) e199.
[28] G. Jiang, J. Yu, J. Wang, et al., Aggregate 3 (2022) e285.
[29] M. Mauro, C. Cebrián, Isr. J. Chem. 58 (2018) 901–914.
[30] J. Wang, X. Gu, H. Ma, et al., Nat. Commun. 9 (2018) 2963.
[31] Z.Q. Chen, Z.Q. Bian, C.H. Huang, Adv. Mater. 22 (2010) 1534–1539.
[32] J. Yin, T. Tao, C. Ou, et al., Dyes Pigm. 205 (2022) 110512.
[33] Y. Ma, J. Yang, S. Liu, et al., Adv. Opt. Mater. 5 (2017) 1700587.
[34] G. Li, Q. Lin, L. Sun, et al., Biomaterials 53 (2015) 285–295.
[35] C. Shi, H. Sun, X. Tang, et al., Angew. Chem. Int. Ed. 52 (2013) 13434–13438.
[36] J. Zhao, K. Yan, G. Xu, et al., Adv. Funct. Mater. 31 (2020) 2008325.
[37] Q. Zhao, F. Li, C. Huang, Chem. Soc. Rev. 39 (2010) 3007–3030.
[38] M.A. Bryden, F. Millward, T. Matulaitis, et al., J. Org. Chem. 88 (2023) 6364–6373.
[39] P.C. Raichure, V. Kachwal, I.R. Laskar, Molecules 27 (2021) 202.
[40] H. Jung, M. Hong, M. Marchini, et al., Chem. Sci. 12 (2021) 9673–9681.
[41] X. Yang, G. Zhou, W.Y. Wong, Chem. Soc. Rev. 44 (2015) 8484–8575.
[42] L. Zu, X. Qian, S. Zhao, et al., J. Am. Chem. Soc. 144 (2022) 2208–2217.
[43] Q. Chen, C. Jin, X. Shao, et al., Small 14 (2018) e1802166.
[44] H. Huang, L. Yang, P. Zhang, et al., Biomaterials 83 (2016) 321–331.
[45] J.S. Choi, A. Maity, T. Gray, et al., J. Biol. Chem. 290 (2015) 9714–9726.
[46] S. Jia, W. Wang, S. Qin, et al., Chin. Chem. Lett. 34 (2023) 107517.
[47] S. Luo, C. Liang, Q. Zhang, et al., Chin. Chem. Lett. 34 (2023) 107666.
[48] S. Liu, J. Han, Y. Chang, et al., Chem. Commun. 58 (2022) 10056–10059.
[49] K. Yang, Y. Zhou, Y. Wang, et al., Chem. Asian J. 16 (2021) 1780–1785.
[50] Y. Li, S. Liu, H. Ni, et al., Angew. Chem. Int. Ed. 59 (2020) 12822–12826.
[51] J. Wang, X. Gu, P. Zhang, et al., J. Am. Chem. Soc. 139 (2017) 16974–16979.
[52] Y. Wu, H.Z. Sun, H.T. Cao, et al., Chem. Commun. 50 (2014) 10986–10989.
[53] R.D. Costa, E. Orti, H.J. Bolink, et al., Angew. Chem. Int. Ed. 51 (2012) 8178–8211.
[54] G.G. Shan, H.-B. Li, H.Z. Sun, et al., J. Mater. Chem. C 1 (2013) 1440–1449.
[55] K.Y. Zhao, H.T. Mao, L.L. Wen, et al., J. Mater. Chem. C 6 (2018) 11686–11693.
[56] X. Li, Y. Yin, H. Yan, et al., Dalton Trans. 46 (2017) 10082–10089.
[57] M.J. Frisch, G.W. Trucks, H.B. Schlegel, et al., Gaussian 09, Revision D.01, Gaussian, Inc., Wallingford, CT, 2009.
[58] H.C. Su, F.C. Fang, T.Y. Hwu, et al., Adv. Funct. Mater. 17 (2007) 1019–1027.
[59] M. Kasha, H.R. Rawls, M.A. El-Bayoumi, Pure Appl. Chem. 11 (1965) 371–392.
[60] P. Alam, W. He, N.L.C. Leung, et al., Adv. Funct. Mater. 30 (2020) 1909268.